THEORETICAL ANALYSIS OF SPECIMEN COOLING RATE DURING IMPACT FREEZING AND LIQUID-JET FREEZING OF FREEZE-ETCH SPECIMENS

GUNNAR KOPSTAD AND ARNLJOT ELGSAETER
Division of Biophysics, University of Trondheim, Trondheim, Norway,

ABSTRACT We have carried out a theoretical analysis of specimen cooling rate under ideal conditions during impact freezing and liquid-jet freezing. The analysis shows that use of liquid helium instead of liquid nitrogen as cooling medium during impact freezing results in an increase in a specimen cooling rate of no more than 30–40%. We have further shown that when both impact freezing and liquid-jet freezing are conducted at liquid nitrogen temperature, the two methods give approximately the same specimen cooling rate under ideal conditions except for a thin outer layer of the specimen. In this region impact freezing yields the highest cooling rate.

INTRODUCTION

The importance of a high cooling rate during freezing of specimens for freeze-etch electron microscopy has long been recognized (Moor, 1964). An increased cooling rate results in reduced average ice crystal size and specimens frozen using the technique that yields the smallest average ice crystal size normally give rise to the most useful electron micrographs. Because the relationship between average ice crystal size and cooling rate is known (Riehle, 1968; Kopstad and Elgsaeter, 1982), the relative usefulness of different methods for freezing of freeze-etch specimens can be estimated theoretically by calculating the specimen cooling rates achieved by the different freezing techniques.

The two basic methods for obtaining high cooling rates during specimen freezing are: (*a*) dropping the specimen onto the surface of a solid conductor at low temperature (impact freezing), (*b*) bringing the specimen instantaneously into thermal contact with a liquid at low temperature and subsequently maintaining a high relative velocity between the liquid and the specimen (spray freezing and liquid-jet freezing). Over the last few years the first approach has received strong renewed interest, particularly as the result of a series of studies by Heuser and coworkers. (Heuser et al., 1979; Heuser and Salpeter, 1979). Also interest in liquid-jet freezing has been increasing (Mueller et al., 1980).

The main purpose of this paper is to establish theoretically the relative performance of impact freezing and liquid-jet freezing under ideal conditions. This has not been done previously. To establish whether or not further efforts to make experimental improvements of these two methods can be expected to be worthwhile such information is crucial. For one special case we have succeeded in deriving the exact mathematical description of the time-dependent specimen temperature distribution during impact freezing. This has not previously been achieved. A preliminary report on this work has appeared elsewhere (Elgsaeter et al., 1980.

GLOSSARY

- A cross-section area of the liquid jet.
- B time-independent parameter determined by Eq. 25.
- C_i (i = 1, 2, and 3) heat capacity of the three phases, solid conductor, frozen specimen, and aqueous specimen.
- C_L heat capacity of the liquid jet.
- $J(t)_\infty$ heat flow removed by the liquid jet for jet velocity $v = \infty$ (m/s).
- K_i (i = 1, 2, and 3) thermal conductivity of the three phases, solid conductor, frozen specimen, and aqueous specimen.
- P initial pressure of the liquid jet.
- T absolute temperature.
- T_c initial temperature of the solid conductor (impact freezing).
- $T_A(t)$ temperature at the liquid jet metal foil interface.
- T_f specimen freezing temperature.
- $T_i(t)$, $T_i'(t)$ temperature at the solid conductor frozen specimen interface (both impact and jet freezing). The prime indicates that T_i is associated with the linearization method (impact freezing).
- T_L temperature of the liquid jet.
- T_s initial temperature of the specimen.
- t time.
- $V(\delta)$ consumed liquid jet volume.
- v liquid jet velocity.
- v_{crit} critical jet velocity.
- x position coordinate of the one-dimentional analyses.
- β, β' time-independent parameter determined by Eqs. 11 and 20, respectively.
- γ, τ' time-independent parameters determined by Eqs. 8 and 16, respectively.

Dr. Kopstad's current address is the Department of Pathology, Regional Hospital N-7000 Trondheim, Norway.

Δ thickness of the solid conductor (liquid jet freezing).

$\delta(t), \delta'(t)$ thickness of the frozen specimen (phase 2). The prime indicates that δ is associated with the linearization method (impact freezing).

ζ heated length of the solid conductor (impact freezing, linearization method).

λ specimen heat of fusion.

ξ mathematical expression given by Eq. 8.

ρ liquid-jet density.

ϕ heat of evaporation of the liquid jet.

THEORY

We have previously shown that when an aqueous specimen is frozen by cooling the whole specimen at the same, high-cooling rate, the specimen solidifies within a temperature interval of only 2–3°C and that the solidification temperature as well as the resulting ice crystal size distribution are determined by the specimen cooling rate (Kopstad and Elgsaeter, 1982). To determine the average ice crystal size in different parts of a specimen exposed to a given specimen freezing technique one must therefore calculate the cooling rate at the solidification temperature of the different parts of the specimen. The full mathematical analysis of this problem is very complex. This is partly so because the specimen solidification temperature itself is cooling-rate dependent and partly because of restraints on how fast the solidification zone can migrate through the specimen due to the temperature-dependent ice crystal growth rate. The main objective of this study is to estimate theoretically the relative usefulness of impact freezing and liquid-jet freezing carried out under various ideal conditions and not to obtain the exact mathematical description of the freezing process. To achieve our objective we will make several simplifications, but the same simplifications will be used in the analysis of both impact freezing and liquid-jet freezing. We will, for instance, ignore the cooling-rate dependence of the specimen solidification temperature as well as the effects of temperature-dependent ice crystal growth rate.

Impact Freezing

The main events of impact freezing are illustrated schematically in Fig. 1. By dropping the specimen onto the surface of a solid conductor the specimen is at time $t = 0$ assumed to be brought instantaneously into full thermal contact with the solid conductor. The thermal contact between the specimen and the solid conductor is assumed to remain unchanged for $t \geq 0$.

For mathematical simplicity we will carry out the analysis in one dimension only and assume that both the specimen and the solid

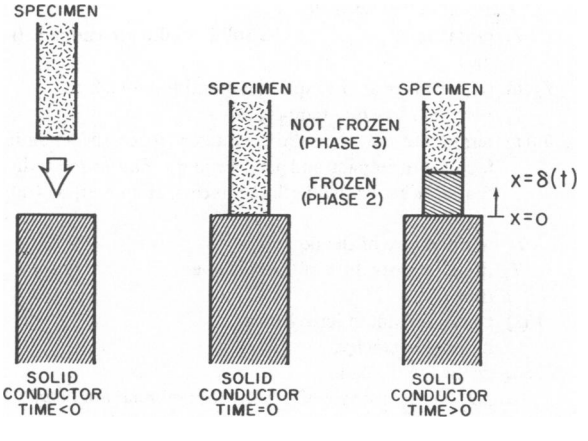

FIGURE 1 A schematic illustration of the main events of impact freezing.

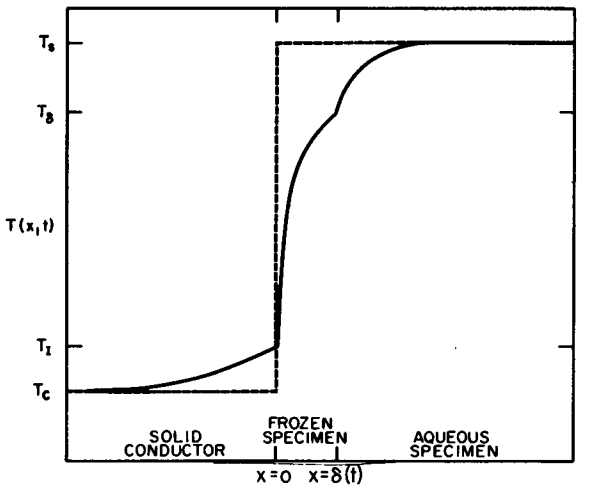

FIGURE 2 A qualitative illustration of the temperature distribution during impact freezing. Time = 0 (– – –), Time > 0 (——).

conductor are infinitely long. Initial conditions at $t = 0$ (Fig. 2) are

$$\text{solid conductor } (x\epsilon < \leftarrow, 0]): T(x, 0) = T_c$$

$$\text{specimen } (x\epsilon < 0, \rightarrow >): T(x, 0) = T_s$$

where x is the position coordinate and $T(x, t)$ is the temperature. For $t > 0$ there will be three phases (Fig. 1):

phase 1 (solid conductor, $x\epsilon < \leftarrow, 0]$): $T(x, t) = T_1(x, t)$

phase 2 (frozen specimen, $x\epsilon < 0, \delta(t)]$): $T(x, t) = T_2(x, t)$

phase 3 (not frozen specimen, $x\epsilon < \delta(t), \rightarrow >$): $T(x, t) = T_3(x, t)$.

The phase number will be used as index to indicate the phase also for thermal conductivity, K [W/(°C m)], and heat capacity, C [Ws/°C m^3)]. For mathematical simplicity K_i and C_i ($i = 1, 2, 3$) are assumed temperature independent. The boundary conditions at the interface between phase 1 and phase 2 ($x = 0$) are

$$T_I = T_1(0, t) = T_2(0, t);$$

$$K_1 \frac{\partial}{\partial x} T_1(0, t) = K_2 \frac{\partial}{\partial x} T_2(0, t). \quad (1)$$

The boundary conditions at the interface between phase 2 and phase 3 [$x = \delta(t)$] are

$$T_2[\delta(t), t] = T_3[\delta(t), t] = T_s$$

$$K_2 \frac{\partial}{\partial x} T_2[\delta(t), t] = K_3 \frac{\partial}{\partial x} T_3[\delta(t), t] + \lambda \frac{d}{dt} \delta(t) \quad (2)$$

where T_s is the specimen freezing temperature (T_s = constant) and λ is the specimen heat of fusion [Ws/m^3].

The temperature distribution in each of the three phases will be fully determined by the initial conditions, the boundary conditions and the following three differential equations:

$$\frac{\partial^2}{\partial x^2} T_i(x, t) = \frac{C_i}{K_i} \frac{\partial}{\partial t} T_i(x, t) \qquad (i = 1, 2, 3). \quad (3)$$

We have succeeded in deriving the exact solution of the mathematical problem specified above. The solution is closely related to the Neumann solution for solidification of a half space (Özişik, 1980):

$$T_1(x, t) = (T_i - T_c)\,(1 + Erf[\sqrt{C_1}\,x/\sqrt{4K_1 t}]) + T_c \qquad (4)$$

$$T_2(x, t) = (T_i - T_\delta)\left[1 - \frac{Erf(\sqrt{C_2}\,x/\sqrt{4K_2 t})}{Erf(\sqrt{C_2}\,\gamma/\sqrt{4K_2})}\right] + T_\delta \qquad (5)$$

$$T_3(x, t) = (T_s - T_\delta)\left[1 - \frac{1 - Erf(\sqrt{C_3}\,x/\sqrt{4K_3 t})}{1 - Erf(\sqrt{C_3}\,\gamma/\sqrt{4K_3})}\right] + T_\delta \qquad (6)$$

where $Erf(u) = 2/\sqrt{\pi}\int_0^u e^{-v^2}dv$. Note that γ is λ-dependent. The temperature at the solid conductor-frozen specimen interface, T_i, can be obtained from Eqs. 1, 4, and 5

$$T_i = (T_\delta - T_s) \cdot [1 + \sqrt{C_1K_1(C_2K_2)}\,Erf(\sqrt{C_2}\gamma/\sqrt{4K_2})]^{-1} + T_c. \qquad (7)$$

The time independence of T_i is a mathematical consequence of the ideal initial conditions. For the ideal conditions described above, the solid conductor and specimen surface instantaneously after impact ($t = 0$) assume the interface temperature T_i.

The time-independent parameter γ is determined by the following transcendental equation (from Eqs. 2, 5, and 6):

$$\frac{\sqrt{C_2K_2}\,(T_\delta - T_i)\exp[-C_2\gamma^2/(4K_2)]}{Erf(\sqrt{C_2}\,\gamma/\sqrt{4K_2})} - \frac{\sqrt{C_3K_3}\,(T_s - T_\delta)\exp[-C_3\gamma^2/(4K_3)]}{1 - Erf[\sqrt{C_3}\,\gamma/\sqrt{4K_3}]} = \frac{\sqrt{\pi}}{2}\gamma\lambda. \qquad (8)$$

The temperature distribution for $t > 0$ for impact freezing is qualitatively illustrated in Fig. 2. The thickness, $\delta(t)$, of phase 2 (frozen specimen) obtained using Eq. 5 and the requirement that $T_2[\delta(t), t] = T_s$ = constant

$$\delta(t) = \gamma t^{1/2}. \qquad (9)$$

The cooling rate at $x = \delta(t)$ is given by

$$\frac{d}{dt}T_2[x = \delta(t), t] = -\beta\,\delta(t)^{-2} \qquad (10)$$

where β is a time independent parameter.

$$\beta = (T_\delta - T_c)\sqrt{C_2/(4\pi K_2)} \cdot \frac{\gamma^3 \exp[-C_2\gamma^2/(4K_2)]}{Erf(\sqrt{C_2}\gamma/\sqrt{4K_2}) + \sqrt{C_2K_2/(C_1K_1)}}. \qquad (11)$$

Numerical values of γ and β are shown in Fig. 3 and Fig. 4 respectively. The following numerical values were used to carry out the calculations:

$C_1 = 3.24 \times 10^6$ [Ws/°C m^3)]; $K_1 = 4.01 \times 10^2$ [W/°C m)]

$C_2 = 1.74 \times 10^6$ [Ws/°C m^3)]; $K_2 = 0.0218 \times 10^2$ [W/°C m)]

$C_3 = 4.20 \times 10^6$ [Ws/°C m^3)]; $K_3 = 0.0574 \times 10^2$ [W/°C m)]

$\lambda = 3.00 \times 10^8$ [Ws/m^3].

These values of C_1 and K_1, C_2 and K_2, and C_3 and K_3 correspond, respectively, to copper at 200°K, ice at 250°K, and water at 273°K (Washburg, 1926; West 1977). These numerical values constitute reasonable estimates of the average values of the respective parameters for the various phases during impact freezing when $T_s \simeq 190$°K.

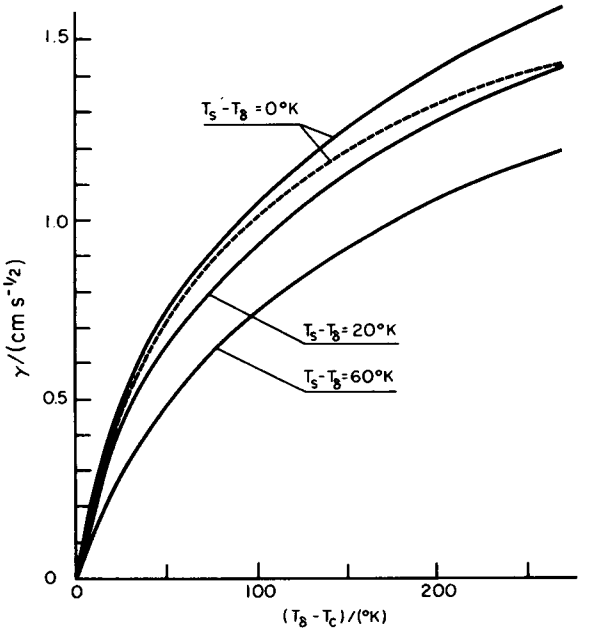

FIGURE 3 Parameter γ for a solid conductor made of copper versus $T_\delta - T_c$ for several values of $T_s - T_\delta$ according to the exact solution (——) and the approximate solution (– – –).

To calculate the specimen cooling rate during jet freezing, we will make use of an approximate method based on linearization of the temperature distribution. We will recalculate the temperature distribution during impact freezing using this temperature linearization approximation for two reasons: (*a*) evaluation of the strength of the temperature linearization approximation by comparing the exact and approximate solutions of the temperature distribution during impact freezing, (*b*) discussion of the effects of changing the experimental conditions, which is much simpler

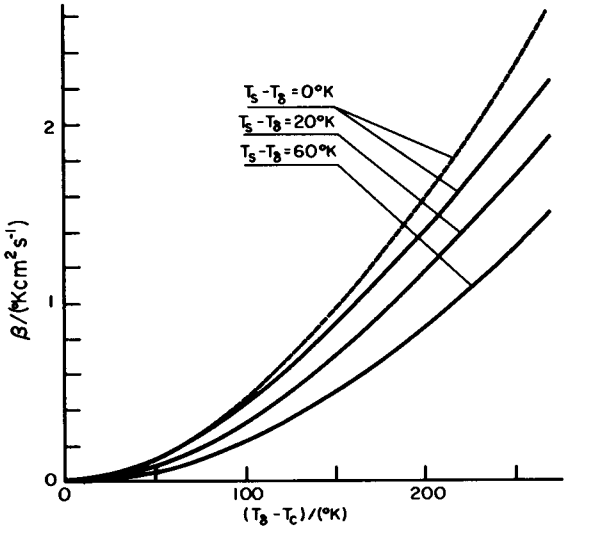

FIGURE 4 Parameter β for a solid conductor made of copper vs. $T_\delta - T_c$ for several values of $T_s - T_\delta$ according to the exact solution (——) and the approximate solution (– – –).

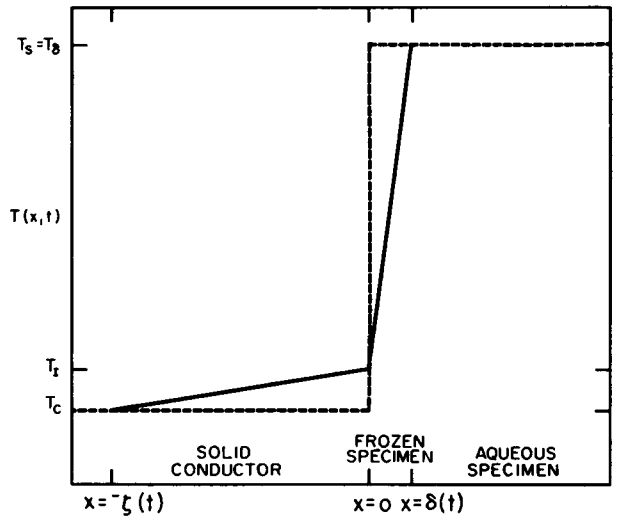

FIGURE 5 Linear approximation of impact freezing temperature distribution. Time = 0 (– – –). Time > 0 (——).

using the approximate rather than the exact solution. The temperature distribution used in the approximate method is shown in Fig. 5. A prime will be used to indicate that a quantity is associated with the approximate method.

$$T_1'(x,t) = \begin{cases} T_c \\ T_c + (T_1' - T_c)(\zeta(t) + x)/\zeta(t) \end{cases}$$

when $x\epsilon < \leftarrow, -\zeta(t)]$

when $x\epsilon < -\zeta(t), 0]$

$$T_2'(x,t) = T_1' + (T_\delta - T_1')\, x/\delta'(t) \qquad \text{when } x\,\epsilon < 0, \delta'(t)]$$

$$T_3'(x,t) = T_\delta = T_s = \text{constant} \qquad \text{when } x\,\epsilon < \delta'(t), \rightarrow >.$$

Heat flow continuity at $x = 0$ yields

$$K_1 \frac{T_1' - T_c}{\zeta(t)} = K_2 \frac{T_\delta - T_1'}{\delta(t)} \tag{12}$$

$$K_2 \frac{T_\delta - T_1'}{\delta'(t)} = \frac{d}{dt}\left\{\int_0^{\delta'(t)} C_2[T_\delta - T_2'(x,t)]\, dx + \delta'(t)\right\}. \tag{13}$$

Energy conservation yields

$$\int_{-\zeta(t)}^{0} C_1 [T_1'(x,t) - T_c]\, dx = \int_0^{\delta'(t)} C_2 [T_\delta - T_2'(x,t)]\, dx + \delta'(t)\,\lambda. \tag{14}$$

Eqs. 12, 13, and 14 yield

$$\delta'(t) = \gamma' t^{1/2} \tag{15}$$

where

$$\gamma' = 2\left(\frac{K_2 (T_\delta - T_1')}{C_2 (T_\delta - T_1') + 2\lambda}\right)^{1/2} \tag{16}$$

$$T_1' = (T_\delta - T_c)\xi + T_c \tag{17}$$

$$\xi = \frac{\sqrt{C_2K_2/(C_1K_1)}}{1 + \sqrt{C_2K_2/(C_1K_1)}} \cdot \frac{1 - \sqrt{\frac{C_1K_1}{C_2K_2}\left(1 + \frac{2\lambda/C_2}{T_\delta - T_c}\right) + \left(\frac{\lambda/C_2}{T_\delta - T_c}\right)^2} + \frac{\lambda/C_2}{T_\delta - T_M}}{1 - \sqrt{C_1K_1/(C_2K_2)}} \tag{18}$$

The cooling rate at $x = \delta'(t)$ is given by

$$\frac{d}{dt} T_2'[x = \delta'(t), t] = -\beta'\delta'(t)^{-2} \tag{19}$$

$$\beta' = (T_\delta - T_c)(1 - \xi)\gamma'^2/2 = (T_\delta - T_1')\gamma'^2/2. \tag{20}$$

Parameters γ' and β' are calculated using the same values for heat capacity, heat conductivity and heat of fusion as in the calculation of γ and β, are shown in Figs. 3 and 4. The same numerical values were used to calculate the heat flow through the solid conductor-frozen specimen interface (Fig. 6) and the time needed to freeze the specimen to depth δ from this interface (Fig. 7).

Liquid-Jet Freezing

The main events of liquid-jet freezing are illustrated schematically in Fig. 8. At time $t = 0$ the liquid-jet is assumed to be instantaneously brought into full thermal contact with the metal foil. The thermal contact between the liquid jet and the metal foil as well as between the metal foil and the specimen is assumed to be unchanged for $t \geq 0$.

For mathematical simplicity the analysis will be carried out in one dimension only and using the linearization approximation method used as an alternative method in the analysis of impact freezing. For time $t < 0$

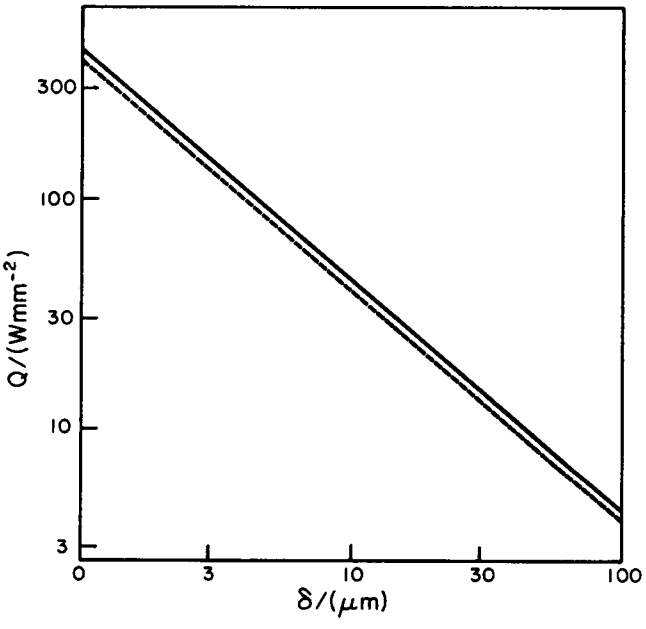

FIGURE 6 Impact freezing heat flow, Q, through the solid conductor-specimen interface according to the exact solution (——) and the approximate solution (– – –) for $T_c = 77°K$, $T_\delta = T_s = 273°K$ and the solid conductor being copper.

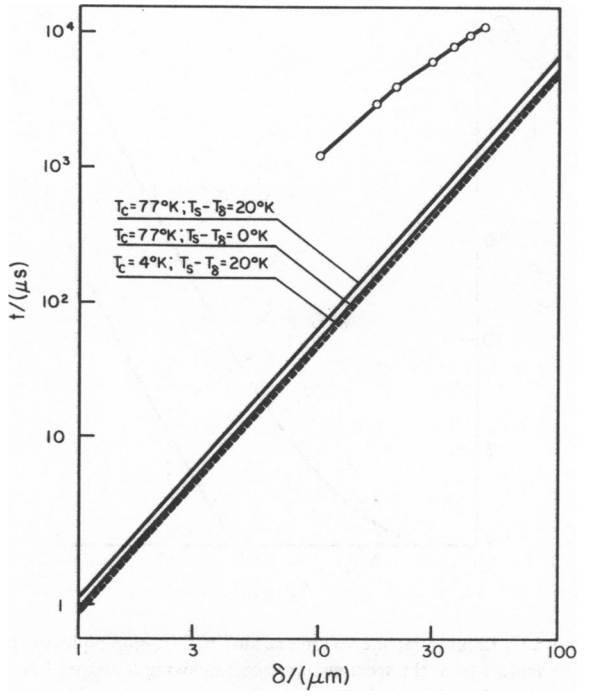

FIGURE 7 Time, t, needed to freeze the specimen to depth δ from the solid conductor-specimen interface to impact freezing with copper as the solid conductor. The lines show the exact solution and the circles the experimental values reported by Heuser et al., 1979.

there will be four phases (Fig. 9):

phase 0 (liquid jet, $x\epsilon < \leftarrow, -\Delta)] : T(x, t) = T_0(x, t)$

phase 1 (solid conductor, $x\epsilon < -\Delta, 0]) : T(x, t) = T_1(x, t)$

phase 2 (frozen specimen, $x\epsilon < 0, \delta(t)]) : T(x, t) = T_2(x, t)$

phase 3 (unfrozen specimen,

$$x\epsilon < \delta(t), \rightarrow >) : T(x, t) = T_3(x, t)$$

$$T_0(x, t) = T_L$$

$$T_1(x, t) = T_\Delta(t) + [T_1(t) - T_\Delta(t)](\Delta + x)/\Delta$$

$$T_2(x, t) = T_1(t) + [T_\delta - T_1(t)]\, x/\delta(t)$$

$$T_3(x, t) = T_\delta.$$

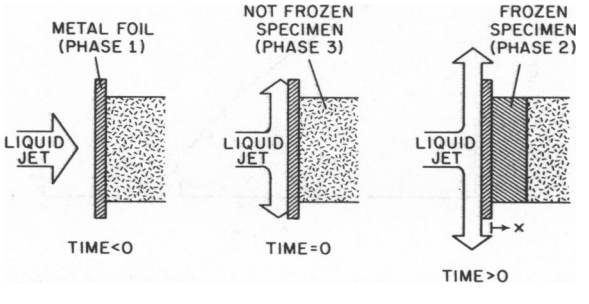

FIGURE 8 A schematic illustration of the main events of liquid-jet freezing.

Provided that T_Δ is not higher than the boiling point of jet liquid and assuming that all the liquid leaving the metal foil has temperature T_Δ the heat flow continuity equation at $x = -\Delta$ is given by

$$vC_L(T_\Delta - T_L) = K_1(T_1 - T_\Delta)/\Delta \tag{21}$$

where v = jet velocity (m/s) C_L = jet liquid heat capacity [Ws/°C m^3)]. Heat flow continuity at $x = 0$ yields

$$K_1(T_1 - T_\Delta)/\Delta = K_2(T_\delta - T_1)/\delta. \tag{22}$$

Energy conservation during liquid-jet freezing yields

$$K_1(T_1 - T_\Delta)/\Delta = \frac{d}{dt}\{\tfrac{1}{2} C_1\Delta[2T_\delta - T_1(t) - T_\Delta(t)] + \tfrac{1}{2} C_2[T_\delta - T_1(t)]\delta + \lambda\delta\}. \tag{23}$$

Eqs. 21, 22, and 23 yield

$$\frac{d}{dt} T_2[x = \delta(t), t] = -B(\delta) \cdot \delta^{-2} \tag{24}$$

$$B(\delta) = \left\{\frac{1}{2} C_2\left[\left(1 + 2\frac{K_1}{\Delta v C_L}\right)\frac{C_1K_2}{C_2K_1}\left(\frac{\Delta}{\delta}\right)^2 + 2\left(1 + \frac{K_1}{\Delta v C_L}\right)\frac{K_2\Delta}{K_1\delta} + 1\right] + \lambda\left[1 + \left(1 + \frac{K_1}{\Delta v C_L}\right)\frac{K_2\Delta}{K_1\delta}\right]^2\right\}^{-1} \cdot K_2(T_\delta - T_L)^2. \tag{25}$$

Some numerical examples calculated using Eq. 24 are shown in Fig. 10; then assume that the liquid jet consists of liquid propane at 83°K with $C_L = 1.1 \times 10^6$ [Ws/(°C m^3)] (Schäfer and Lax, 1961).

Instead of boundary conditions Eqs. 22 and 23 one may use

$$K_1(T_1 - T_\Delta)/\Delta = K_2(T_\delta - T_1)/\delta + \frac{d}{dt}\left[\frac{1}{2} C_1(2T_\Delta - T_1 - T_\Delta)\Delta\right] \tag{26}$$

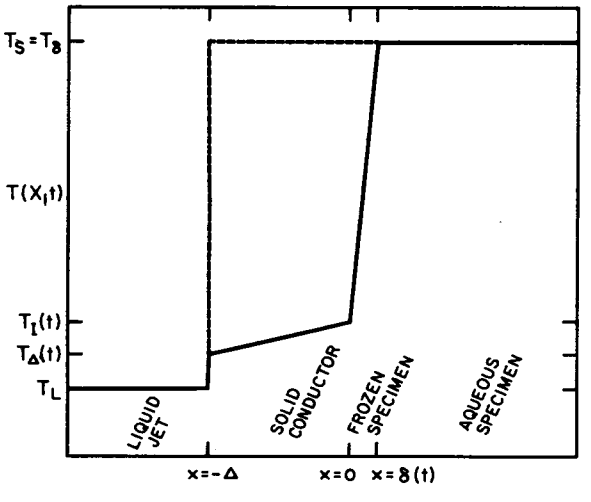

FIGURE 9 Temperature distribution used to calculate the thermal behavior during liquid-jet freezing. Time = 0 (– – –). Time > 0 (——).

$$K_2(T_\delta - T_1)/\delta = \frac{d}{dt}\left[\frac{1}{2}C_2(T_\delta - T_1)\delta + \lambda\delta\right]. \quad (27)$$

This choice of boundary conditions does not, however, yield an analytical expression for the cooling rate. Using numerical methods we have also carried out a detailed analysis using boundary conditions Eqs. 26 and 27. The cooling rates obtained employing the latter boundary conditions deviate at most a few percent from the values shown in Fig. 10.

The consumed liquid jet volume V for liquid jet and specimen with cross-section area A is given by

$$V(\delta) = v \cdot t(\delta) \cdot A \quad (28)$$

The results depicted in Fig. 11 were obtained by calculating numerically $t = t(\delta)$ for $v = 6$ and 60 (m/s).

In the derivation above it was assumed that T_Δ was lower than the boiling point of the liquid jet. However, liquids at their boiling point, such as liquid nitrogen, may also be of interest as the fluid of the liquid jet. In this case cooling will, for sufficiently large v, originate mainly from the heat of evaporation, ϕ, of the component of the liquid jet. The heat flow $J(t)_\infty$, at $x = -\Delta$ for jet velocity $v = \infty$ (m/s) ($T_\Delta = T_L$) can be obtained from Eqs. 22 and 23. For jet velocity v larger than a certain critical velocity, v_{crit}, the liquid jet will be capable of removing the heat given by $J(t)_\infty$. Provided that the jet becomes fully vaporized as it hits the metal foil ($x = -\Delta$) the heat flow continuity equation at $x = -\Delta$ gives

$$J(t)_\infty = v_{crit}(t) \cdot \phi = K_1[T_1(t) - T_L]/\Delta. \quad (29)$$

The relationship between liquid jet initial pressure, P, and jet velocity equals

$$P = \tfrac{1}{2}\rho v^2 \quad (30)$$

when ρ is the density of the liquid jet. Using Eqs. 22, 23, 29, and 30 P_{crit} have been calculated using $\phi = 1.6 \times 10^{+8}$ (Ws/m^3), which corresponds to liquid nitrogen (West, 1977), and copper metal foil with thickness $\Delta = 30$ μm. The result of this numerical calculation is given in Fig. 12.

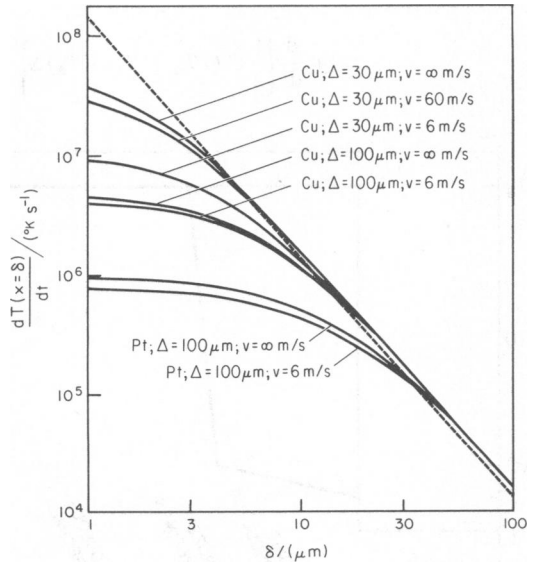

FIGURE 10 Specimen cooling rate at $x = \delta$ during liquid-jet freezing using liquid propane. $T_L = 83$°K and $T_s = T_\delta = 273$°K (——). Cooling rate at $x = \delta$ during impact freezing when $T_c = 77$°K, $T_s = T_\delta = 273$°K and copper is used as solid conductor (– – –).

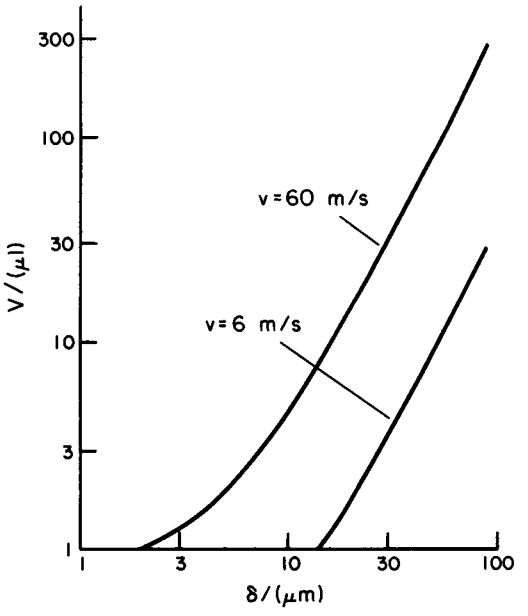

FIGURE 11 Liquid propane volume needed to freeze an aqueous specimen to depth δ from the specimen surface employing liquid-jet freezing. $T_L = 83$°K, $T_s = T_\delta = 273$°K. $A = 1$ mm^2. Metal foil, 30 μm thick copper.

DISCUSSION

The theoretical analysis we have conducted rests on several assumptions. One of these is that the specimen at time $t = 0$ during impact freezing instantaneously comes into full thermal contact with the solid conductor and that the thermal contact remains unchanged for $t \geq 0$. We have previously carried out experiments that indicate that this may be an unrealistic assumption, particularly for nonviscous specimens (Elgsaeter et al., 1980). This conclusion is supported by the measurements of the time, t, needed to freeze a specimen to a given depth (Heuser et al., 1979) and shown in Fig. 7. The experimentally determined values of t are 10–30 times larger than the values predicted by the theoretical analysis of impact freezing under ideal condi-

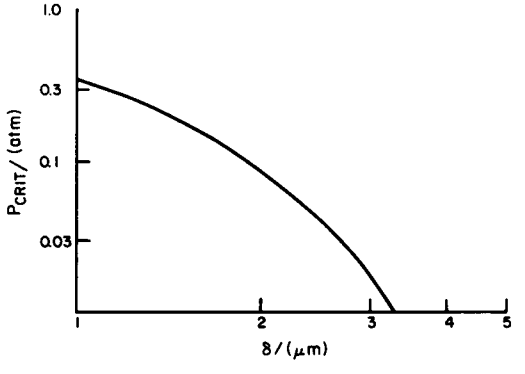

FIGURE 12 Critical pressure, P_{crit}, vs. $\delta(t)$ during liquid-jet freezing using liquid N_2 at its boiling point to freeze an aqueous specimen. Metal foil, 30 μm thick copper.

tions. During impact freezing as well as liquid-jet freezing the part of the specimen facing the solid conductor may be cooled down 150–200 (°K) after it has solidified. This results in significant contraction of the solidified specimen and mechanical strain on the mechanical contact between the solid conductor and the frozen specimen. Any slippage at the solid conductor–specimen interface introduces non-idealities in the thermal contact at the interface. The calculated cooling rates therefore are the highest obtainable values.

In the theoretical analysis of impact freezing, both the solid conductor and the specimen were assumed to be of infinite length. From Eqs. 12 and 17 it is seen that $\zeta(t)/\delta(t) \approx 1.5[(C_2/K_2)/(C_1/K_1)]^{1/2} \simeq 15$ for impact freezing at liquid nitrogen or lower temperature using copper as solid conductor. For a copper conductor being several centimeters long the assumption that both the solid conductor and specimen are infinitely long therefore only introduces minor errors in the specimen cooling rate for specimen thickness less than a few millimeters.

In standard setups for impact freezing (Heuser et al., 1979) the diameter of the solid conductor is several times the diameter of the specimen. During impact freezing there will therefore also be a certain radial heatflow in the solid conductor. This will give a somewhat reduced $T_I - T_c$, but for impact freezing at liquid nitrogen or liquid helium temperature a reduction of $T_I - T_c$ beyond what results from the one-dimensional analysis, has only a negligible effect (see Eqs. 16 and 20) in specimen cooling rate. Thus, use of a one-dimensional analysis for specimen cooling rates during impact freezing yields reasonably accurate estimates under the freezing conditions of most interest, i.e., for low values of T_c.

In the theoretical analysis it was assumed that both the heat capacity and the thermal conductivity of the different phases during impact freezing were temperature independent. This is generally not the case. Except for possible anomalies because of phase transitions, the heat capacity of solids generally decreases as the temperature is decreased. At liquid helium temperature the heat capacity of most solids is <0.1% of the value at room temperature (Kittel, 1967). The thermal conductivity of pure metals and thermal conductors such as sapphire (Al_2O_3) and diamond exhibits a maximum at 40–100°K (Kittel, 1967). As the temperature is reduced further towards liquid helium temperature, the thermal conductivity of these conductors also drops sharply. Reasonably accurate estimates of the specimen cooling rate during impact freezing at liquid nitrogen temperature can be achieved using the thermal conductivity and heat capacity of the solid conductor at liquid nitrogen temperature and the average value of ice thermal conduction and heat capacity in the temperature interval 80–273°K in the theoretically derived expressions. This procedure, however, does not work for impact freezing at liquid helium temperature. The reason for this is the strong temperature dependence of the thermal conductivity, K, and heat capacity, C, of all solid conductors of interest in the temperature interval between liquid helium temperature and 30–60°K.

If the values of C and K for, say, copper for all temperatures equalled the values at 4°K, the interface temperature T_I would assume a value closer to T_s than T_c instantaneously after impact and thus yield a low value of the specimen cooling rate in spite of the very low value of T_c. However, as T_I on its instantaneous approach to a value near T_s reaches 30–40°K the values of C and K for the solid conductor surface layer no longer correspond to such a high value of T_I, and T_I will not increase further during its instantaneous increase for $t = 0$ than is predicted by the developed theory when $T_c \simeq 30$–40°K. That is, nothing is to be gained in specimen cooling rate under ideal conditions by using $T_c = 4$°K instead of 30–40°K for all known types of solid conductors.

Ultra high-purity copper is often used as solid conductor in impact freezing (Heuser et al., 1975). From Eqs. 16 and 20 it is seen that the specimen cooling rate during impact freezing at liquid nitrogen and liquid helium temperature is essentially proportional to $(T_\delta - T_I')^{1.5}$ for a given value of δ. Eqs. 17 and 18 further show that for standard electrolytic copper as solid conductor during impact freezing at liquid nitrogen temperature or lower, T_I' is already so close to T_c that no more than 10–15% is to be gained in specimen cooling rate even by using a solid conductor with $C \cdot K = \infty$ [$W^2s/(°C^2m^4)$]. Because a 10% increase in cooling rate results in no more than 10–15% reduction in average specimen ice crystal size (Kopstad and Elgsaeter, 1982), use of ultra high purity copper, diamond, or sapphire as solid conductor instead of standard electrolytic copper only gives a marginal reduction in average ice-crystal size.

Liquid helium has been used as the cooling liquid in most recent studies using impact freezing (Heuser et al., 1979; Heuser and Salpeter, 1979). It was pointed out above that for a given value of δ, the cooling rate essentially is propotional to $(T_\delta - T_I)^{1.5}$ and that when copper is used as solid conductor $T_I' \approx T_c$. During impact freezing at liquid nitrogen temperature $T_c \simeq 80$°K. For impact freezing at liquid helium temperature the effective $T_C \approx$ 30–40°K, which means that $T_\delta - T_I'$ and therefore the specimen cooling rate under ideal conditions, increases 30–40% by doing impact freezing at liquid helium instead of liquid nitrogen temperature. This results in a decrease in average specimen ice-crystal size of no more than 30–60%. The theoretical analysis of impact freezing under ideal conditions thus indicates that the increased expense and complexity of doing impact freezing using liquid He^I or He^{II} as cooling liquid instead of liquid nitrogen therefore hardly seems warranted for most applications.

In the theoretical analysis the specimen solidification temperature T_δ is assumed to be constant. Generally,

however, T_δ will be cooling rate dependent (Kopstad and Elgsaeter, 1982), which means that T_δ is different at different distances from the specimen surface. Figs. 3 and 4, however, show that for impact freezing at liquid nitrogen or liquid helium temperature, the cooling rate at most changes 10–20% as result of changes in T_δ of 20–30°K.

From Fig. 4 it is seen that the specimen temperature only has a minor effect on the resulting specimen cooling rate using impact freezing. By using a specimen temperature of 0°C instead of 20°C only a gain in the cooling rate of 15–20% is obtained.

A striking feature of impact freezing is that the solid conductor-specimen interface temperature, T_I, is constant under ideal conditions. For high jet velocities the jet-metal foil interface temperature, T_Δ, during liquid-jet freezing will also be approximately constant and equal to the jet temperature T_L. For $T_I = T_L$ and values of $\delta \gg \Delta$ it is therefore to be expected that the specimen cooling rate will be the same for impact freezing and liquid-jet freezing. The numerical results presented in Fig. 10 verify that this is the case. In Fig. 10 the liquid-jet cooling rate for large values of δ is somewhat higher than for impact freezing because $T_I > T_L$. For infinitely thin metal foil liquid-jet freezing and impact freezing at liquid nitrogen temperature, for instance, the same cooling rate would be achieved for all values of δ provided that $T_I \approx T_\Delta$. For nonzero metal foil thickness there will be a outer region of the specimen frozen using liquid-jet freezing that has been subjected to a lower cooling rate than a specimen frozen using impact freezing. The specimen cooling rate versus δ for different metal foils and jet velocities using liquid-jet freezing is shown in Fig. 10.

The conclusions of our theoretical analysis of specimen freezing under ideal conditions are (a) no more than 30–40% is to be gained in specimen cooling rate by doing impact freezing at liquid helium temperature instead of at liquid nitrogen temperature, (*b*) except for thin outer layer of the specimen the specimen cooling rates resulting from respectively liquid-jet freezing and impact freezing conducted at the same temperature are approximately equal. Under ideal conditions impact freezing yields the highest cooling rates in the thin outer layer of the specimen.

REFERENCE

Elgsaeter, A., T. Espevik, and G. Kopstad. 1980. Rapid freezing of freeze-etch specimens. 38th Annual Proceedings of Electron Microscopy Society of America. G. W. Baily, editor. Claitor's Publishing Division, San Francisco, CA. 752–755.

Heuser, I. E., T. S. Reese, M. J. Dennis, Y. Jan, L. Jan, and L. Evans. 1979. Synaptic vesicles exocytosis captured by quick freezing and correlated with quantal transmitter release. *J. Cell Biol.* 81:275–300.

Heuser, J. E., T. S. Reese, and D. M. D. Landis. 1975. Preservation of synaptic structures by rapid freezing. *Cold Spring Harbor Symp. Quant. Biol.* 17–24.

Heuser, I. E., and S. R. Salpeter. 1979. Organization of acetylcholine receptors in quick-frozen, deep-etched, and rotary-replicated *Torpedo* postsynaptic membrane. *J. Cell Biol.* 82:150–173.

Kittel, C. 1967. Introduction to Solid State Physics. John Wiley & Sons, Inc., New York. 165–195.

Kopstad, G., and A. Elgsaeter. 1982. A theoretical analysis of the ice-crystal size distribution of frozen aqueous specimens. *Biophys. J.* 40:155–161.

Moor, H. 1964. Die Gefrier-Fixation lebender Zellen und ihr Anwendung in der Elektronenmikroskopie. *Z. Zellforsch. Mikrosk. Anat.* 62:546–580.

Mueller, M., N. Meister, and H. Moor, 1980. Freezing in a propane jet and its application in freeze-fracturing. *J. Microsc. (Wein).* 36:129–140.

Özisik, M.N. 1980. Heat Conduction. John Wiley & Sons, Inc., New York. 397–412.

Riehle, U. 1968. Ueber die Vitrifizierung verdünnter wässiger Lösungen. Diss.n° 4271, Eidgenössische Technische Hochschule Zürich, Juris Druck Verlag, Zürich. 1–133.

Schäfer, K., and E. Lax. 1961. Landolt-Börstein, Zahlenwerte und Funktionen. II Band. 4. Teil. 6. Auflage. Springer-verlag, Berlin. 521.

Washburg, E. W. 1926. International Critical Tables. McGraw-Hill, Inc., New York. 5:217.

West, R. C. 1977. Handbook of chemistry and physics. 58th edition. CRC Press, Inc., West Palm Beach, FL. A1-158.